



## Blind Dereverberation for MRI Acoustic Noise

Hua Bao <sup>1+</sup>, Issa Panahi <sup>1</sup> and Richard Briggs <sup>2</sup>

<sup>1</sup> Department of Electrical Engineering, University of Texas at Dallas, Richardson, Texas, U.S.A.

<sup>2</sup> University of Texas Southwestern Medical Center, Dallas, Texas, U.S.A

**Abstract.** In Magnetic Resonance Imaging (MRI) room, strong acoustic noise during the scan not only creates harmfully annoying environment but also interferes with brain activation response. The presence of reverberation in the MRI environment interferes with efficient noise canceling techniques. In this paper, we present a blind dereverberation method for estimating the broadband MRI acoustic noise signal from the sensor measurements. The method is based on modeling the acoustic noise as an autoregressive (AR) process and using a single input multiple output (SIMO) linear prediction system. In our experiments, we use not only synthetic data but also actual recording of the reverberant MRI acoustic noise signals in a room and in a test-bed mimicking the MRI bore. A criteria based on spectral characteristics is employed to analyze the performance of this method. Experimental results show effective removal of the reverberation from the original noise signal over a broad band of signal spectrum. Results in this paper will provide further help to improve noise cancellation performance in MRI environment.

**Keywords:** MRI acoustic noise, blind dereverberation, active noise control

### 1. Introduction

In Magnetic Resonance Imaging (MRI) system, strong acoustic noise are generated by rapid switching of gradient coil which results in changing Lorentz forces on the gradient coil conductor. The acoustic noise of up to 120 dB SPL (Sound Pressure Level) has been measured in a 3-Tesla MRI room. The acoustic noise signal in a MRI room is a combination of the noise created by the vibration of scanner structure and sounds from the ancillary equipments associated with the MRI system in the room (e.g. cooling Helium pump and fan, ventilation fan). We refer to this noise as the scanner noise herein. Presence of scanner noise in audible range not only creates a detrimentally annoying environment for patients and technicians but also interfere with functional magnetic resonance imaging (fMRI) through direct and indirect ways [1-3]. Direct interference comes with an increase in regional cerebral blood flow, interacting with the blood oxygen level dependent (BOLD) response of the brain activation. Indirect interference exists in the distraction on the perception of the stimulus by strong scanner noise.

To attenuate the interference from scanner noise, passive method are utilized by using earplugs and/or circumaural ear defenders [4]. Adaptive noise control (ANC) [5] methods have been developed and utilized to attenuate the acoustic noise in MRI room [6-7]. However, the scanner noise is mixed with its acoustic reverberation at measuring points in the room. Research indicates that noise attenuation level will be degraded by the increase of reverberation [8]. Contaminating effects and characteristics of the

---

<sup>+</sup> Corresponding author.

E-mail address: [hua.bao@student.utdallas.edu](mailto:hua.bao@student.utdallas.edu) .

reverberation vary as a function of several parameters such as the Echo Planar Imaging (EPI) sequence selected for MRI experiment, acoustic characteristics of the room including the type and shape of different objects present in the room. Therefore, there is a need to separate the noise signal from its reverberation, which is termed as dereverberation.

Dereverberation techniques attempt to recover an original signal from its mix with reverberant components at measurement sensors. This technique has been widely used in speech enhancement [9], damage detection [10], and geophysical exploration [11]. By nature, dereverberation is also a deconvolution problem attempting to remove the reverberant signal from the convolutive mixture of signal components [12, 13]. In general, dereverberation methods can be categorized as two types: white-box methods, and black-box methods. For the white-box approach, the room transfer function (RTF) is required and reverberation is removed by inverse filtering technique [14, 15]. For the black-box approach, also known as blind dereverberation, only the measurements of the reverberant signals are required. Such methods avoid the error introduced by RTF estimation techniques.

In this paper, we apply the LIME method (Linear predictive Multi-input Equalization) [16], a primary black-box method based on Single Input Multiple Output (SIMO) linear prediction, to the blind dereverberation of the MRI acoustic noise. The LIME method is chosen because it has been proven efficient for dereverberating the speech signals. We initially applied LIME method to conduct blind dereverberation for MRI acoustic noises with synthetic reverberation in two cases: noises with and without speech [17]. In this paper, we consider three reverberant signals generated by the actual MRI acoustic noise in our experiments. In the first experiment, we verify the effectiveness of dereverberation for MRI acoustic noise by using ideal reverberant signals generating by image method [18] synthetically. In order to test the dereverberation in realistic environments, we utilize reverberant signals recorded in a test-room and a test-bed mimicking the MRI bore in the second and third experiments.. We employ an efficient algorithm to determine the characteristic polynomial of a large size (>200-by-200) square matrix obtained from the covariance matrices of the measured data. The characteristic polynomial represents an AR model for the dereverberated signal. We also define a criterion based on the power spectra of the original and estimated (dereverberated) source signals in order to evaluate the effectiveness of the proposed blind dereverberation method. Comparing spectral variations of the signals illustrates removal of the reverberation as a function of frequency.

This paper is organized as follows. Section 2 describes the model for the room reverberation and introduces the LIME method that we use for dereverberation. In Section 3, the system setup and results for the three types of experimentations are presented and discussed. The experiments include dereverberation performed on synthetic data, recorded data in the test room and the MRI bore test-bed. Concluding remarks are in Section 4.

## 2. Methods

The dereverberation method for the SIMO system is shown in Fig. 1. The original signal (i.e. the MRI acoustic noise), denoted as  $x(n)$ , is assumed to be an  $N^{\text{th}}$ -order AR process modeled by  $1/A(z)$ , where

$$A(z) = 1 - \sum_{k=1}^N a_k z^{-k}, \quad a_k \text{ is the coefficient of the AR process.}$$

The loudspeaker  $S$  is considered ideally amplifying  $x(n)$  only.  $u_1(n)$  and  $u_2(n)$  are the outputs of microphones (sensors)  $M_1$  and  $M_2$ , respectively, which receive the reverberant signals via  $H_1(z)$  and  $H_2(z)$  - the RTFs of two different acoustic paths. Microphone outputs are the measured data used for our blind dereverberation method to recover (estimate) the original MRI acoustic noise signal. In using the LIME algorithm, similar to that in [16], we assume that: (1) the original signal  $x(n)$  is a finite order AR process, i.e. it is the output of the

LTI all-pole stable system  $1/A(z)$  driven by the stationary zero-mean white noise  $e(n)$ ; (2) the Room Transfer Functions (RTFs)  $H_1(z)$  and  $H_2(z)$  are linear time-invariant FIR filters with no common zeros. This implies that the two microphones  $M_1$  and  $M_2$  should be placed asymmetrically with respect to the original signal source with sufficient spatial distances from each other and the source; (3) we assume  $M_1$  is closer to the noise source than  $M_2$ .

## 2.1. System model and Problem Formulation

In Fig. 1, the error  $\hat{e}(n)$  is obtained by using  $u_1(n-1)$ ,  $u_2(n-1)$  and the prediction filters  $\omega_1(z)$ ,  $\omega_2(z)$ . It will be proven later that  $\hat{e}(n)$  is factually proportional to the white noise  $e(n)$ .  $\hat{A}(z)$  is the estimate of  $A(z)$  polynomial, which is used to obtain the dereverberated signal  $\hat{x}(n)$  by filtering  $\hat{e}(n)$  through  $1/\hat{A}(z)$ . Formulation of the method is as follows. The prediction error is expressed as:

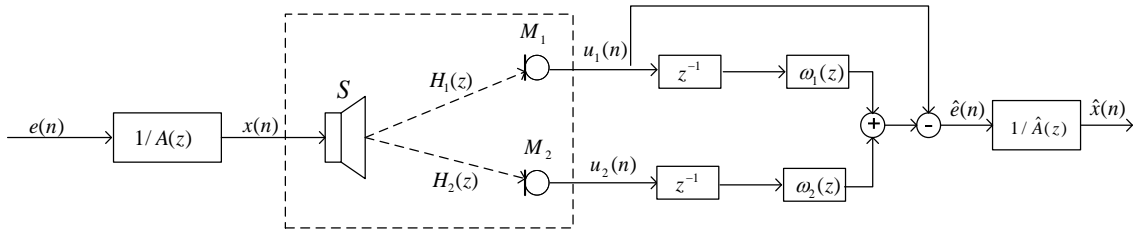


Fig.1: The dereverberation system scheme

$$\begin{aligned}
 \hat{e}(n) &= u_1(n) - (\omega_1(n) * u_1(n-1) + \omega_2(n) * u_2(n-1)) \\
 &= h_1(n) * x(n) - \{\omega_1(n) * h_1(n) * x(n-1) \\
 &\quad + \omega_2(n) * h_2(n) * x(n-1)\} \\
 &= \mathbf{x}_n^T \mathbf{h}_1 - \mathbf{x}_{n-1}^T \mathbf{H} \boldsymbol{\omega}
 \end{aligned} \tag{1}$$

where linear convolution operator is denoted by  $*$ , and row vector  $\boldsymbol{\omega}$  defines coefficients of the prediction filters as  $\boldsymbol{\omega} = [\boldsymbol{\omega}_1^T, \boldsymbol{\omega}_2^T]$ , where  $\boldsymbol{\omega}_i = [\omega_{i,0}, \dots, \omega_{i,L-1}]^T$  and  $\omega_{i,k} \equiv \omega_i(k)$ ,  $i = 1, 2$ .  $L$  is the order of prediction filter  $\boldsymbol{\omega}_i$

$$\mathbf{h}_1 = [h_{1,0}, \dots, h_{1,m-1}, 0, \dots, 0]^T,$$

$$\mathbf{x}_n = [x(n), \dots, x(n - (m + L - 1))]^T,$$

$\mathbf{H}$  is a full row-rank matrix of size  $(m + L) \times 2L$ , where  $2L \geq m + L$ , and  $\mathbf{H} = [\mathbf{H}_1, \mathbf{H}_2]$ .

$\mathbf{H}_i$  is a  $(m + L) \times L$  matrix expressed as

$$\mathbf{H}_i = \begin{bmatrix} h_{i,0} & 0 & \dots & 0 \\ h_{i,1} & h_{i,0} & \ddots & \vdots \\ \vdots & \ddots & \ddots & \\ h_{i,m-1} & & & 0 \\ 0 & h_{i,m-1} & & h_{i,0} \\ \vdots & & \ddots & \vdots \\ 0 & \dots & 0 & h_{i,m-1} \end{bmatrix}, \quad i = 1, 2.$$

By minimizing the mean square value of the prediction error  $\hat{e}(n)$ , we obtain

$$\boldsymbol{\omega} = (\mathbf{H}^T E\{\mathbf{x}_{n-1} \mathbf{x}_{n-1}^T\} \mathbf{H})^+ \mathbf{H}^T E\{\mathbf{x}_{n-1} \mathbf{x}_n^T\} \mathbf{h}_1, \tag{2}$$

where,  $^+$  is the Moore-Penrose generalized inverse of the matrix, and  $E\{\cdot\}$  is the expectation operator. If we replace the column vector  $\mathbf{h}_1$  with matrix  $\mathbf{H}$  in (2), we find matrix  $\mathbf{Q}$  as:

$$\mathbf{Q} = (\mathbf{H}^T E\{\mathbf{x}_{n-1}\mathbf{x}_{n-1}^T\}\mathbf{H})^+ \mathbf{H}^T E\{\mathbf{x}_{n-1}\mathbf{x}_n^T\}\mathbf{H}. \quad (3)$$

Since the input signal is generated by an AR process, we can write  $\mathbf{x}_n = \mathbf{C}^T \mathbf{x}_{n-1} + \mathbf{e}_n$ , where

$\mathbf{e}_n = [e(n), 0, \dots, 0]^T$ , and  $\mathbf{C}$  is the companion matrix given by

$$\mathbf{C} = \begin{pmatrix} a_1 & 1 & 0 & \dots & 0 \\ a_2 & 0 & 1 & \dots & 0 \\ \vdots & \vdots & \ddots & \ddots & \vdots \\ \vdots & \vdots & & \ddots & 1 \\ a_N & 0 & \dots & \dots & 0 \end{pmatrix} \quad (4)$$

We then have:

$$E\{\mathbf{x}_{n-1}\mathbf{x}_n^T\} = E\{\mathbf{x}_{n-1}\mathbf{x}_{n-1}^T\}\mathbf{C} \quad (5)$$

In (5),  $E\{\mathbf{x}_{n-1}\mathbf{x}_{n-1}^T\}$  is the real symmetric positive-definite (state) covariance matrix of the (system) signal, and  $\mathbf{C}$  is the companion real matrix of a LTI causal stable system whose eigenvalues are inside unit circle.

By replacing  $E\{\mathbf{x}_{n-1}\mathbf{x}_{n-1}^T\}$  with  $\mathbf{X}^T\mathbf{X}$ , where  $\mathbf{X} = \frac{1}{\sqrt{m+L}}[\mathbf{x}_{n-1}, \mathbf{x}_{n-2}, \dots, \mathbf{x}_{n-(m+L)}]$ , matrix  $\mathbf{Q}$  can be expressed as:

$$\begin{aligned} \mathbf{Q} &= (\mathbf{H}^T \mathbf{X}^T \mathbf{X} \mathbf{H})^+ \mathbf{H}^T \mathbf{X}^T \mathbf{X} \mathbf{C} \mathbf{H} \\ &= (\mathbf{X} \mathbf{H})^+ \mathbf{X} \mathbf{C} \mathbf{H} \\ &= \mathbf{H}^T (\mathbf{H} \mathbf{H}^T)^{-1} (\mathbf{X}^T \mathbf{X})^{-1} \mathbf{X}^T \mathbf{X} \mathbf{C} \mathbf{H} \\ &= \mathbf{H}^T (\mathbf{H} \mathbf{H}^T)^{-1} \mathbf{C} \mathbf{H} \end{aligned} \quad (6)$$

where, the first column of  $\mathbf{Q}$  defines coefficients of the prediction filters as

$$\boldsymbol{\omega} = \mathbf{H}^T (\mathbf{H} \mathbf{H}^T)^{-1} \mathbf{C} \mathbf{h}_1 \quad (7)$$

Furthermore, the prediction error is obtained as

$$\begin{aligned} \hat{\mathbf{e}}(n) &= \mathbf{x}_n^T \mathbf{h}_1 - \mathbf{x}_n^T \mathbf{H} \boldsymbol{\omega} \\ &= \mathbf{x}_n^T \mathbf{h}_1 - \mathbf{x}_n^T \mathbf{H} \mathbf{H}^T (\mathbf{H} \mathbf{H}^T)^{-1} \mathbf{C} \mathbf{h}_1 \\ &= (\mathbf{x}_n^T - \mathbf{x}_{n-1}^T \mathbf{C}) \mathbf{h}_1 \\ &= \mathbf{e}_n^T \mathbf{h}_1 = h_{1,0} e(n) \end{aligned} \quad (8)$$

As shown in (8), the prediction error  $\hat{\mathbf{e}}(n)$  is proportional to the white noise  $e(n)$ .

## 2.2. Estimation of the AR Model, $1/\hat{A}(z)$

The characteristic polynomial of the companion matrix  $\mathbf{C}$  is

$$\begin{aligned} f_c(\mathbf{C}, \lambda) &= -\lambda^N + a_1 \lambda^{N-1} + \dots + a_N \\ &= -\lambda^N \{1 - (a_1 \lambda^{-1} + \dots + a_N \lambda^{-N})\} \end{aligned} \quad (9)$$

where  $f_c(\mathbf{M}, \lambda) = \det(\mathbf{M} - \lambda \mathbf{I})$  is the characteristic polynomial of matrix  $\mathbf{M}$ . We note that the coefficients of the polynomial  $A(z)$  equal to the coefficients of the characteristic polynomial of matrix  $\mathbf{C}$ . That is, using (6) we obtain

$$\lambda(\mathbf{Q}) = \lambda(\mathbf{H}^T (\mathbf{H} \mathbf{H}^T)^{-1} \mathbf{C} \mathbf{H}) = \lambda(\mathbf{H} \mathbf{H}^T (\mathbf{H} \mathbf{H}^T)^{-1} \mathbf{C}) = \lambda(\mathbf{C}) \quad (10)$$

where  $\lambda(\mathbf{Q})$  means eigenvalues of matrix  $\mathbf{Q}$ . We can thus derive that:

$$f_c(\mathbf{Q}, \lambda) = f_c(\mathbf{C}, \lambda) \quad (11)$$

Therefore, the estimated polynomial  $\hat{A}(z)$  can be obtained from the characteristic polynomial of matrix  $\mathbf{Q}$ , and that the roots of  $\hat{A}(z)$  are inside the unit circle.

### 2.3. Matrix Q Calculation

Matrix  $\mathbf{Q}$  is important for obtaining the dereverberated signal. But as seen in (3),  $\mathbf{Q}$  is expressed in terms of original signal  $x(n)$ . To implement the blind dereverberation, only the output of the microphones  $u_1(n)$  and  $u_2(n)$  are available for use. Therefore, we will express  $\mathbf{Q}$  in terms of  $u_1(n)$  and  $u_2(n)$  as follows. We write

$$\mathbf{u}_n = \mathbf{H}^T \mathbf{x}_n \quad (12)$$

where,  $\mathbf{u}_n = [u_1(n) \ \dots \ u_1(n-L+1) \ u_2(n) \ \dots \ u_2(n-L+1)]^T$ .

Then using (12), we obtain from (3) that

$$\mathbf{Q} = (E\{\mathbf{u}_{n-1} \mathbf{u}_{n-1}^T\})^{-1} E\{\mathbf{u}_{n-1} \mathbf{u}_n^T\} \quad (13)$$

Using the above dereverberation, we formalize our algorithm as in the next subsection.

### 2.4. Blind Dereverberation Algorithm

Flowchart of the blind dereverberation algorithm is shown in Fig. 2. The algorithm requires the following six steps:

- 1) Matrix  $\mathbf{Q}$  is estimated using the two signals received at the microphones as in (13),
- 2) Coefficients of the prediction filters,  $\omega_1$  and  $\omega_2$ , are given by the first column of matrix  $\mathbf{Q}$ ,
- 3) Prediction error is calculated using the first equation in (1),
- 4) Compute the characteristic polynomial of  $\mathbf{Q}$ .
- 5) Coefficients of polynomial  $\hat{A}(z)$  are coefficients of the characteristic polynomial of  $\mathbf{Q}$ ,
- 6) Dereverberated signal,  $\hat{x}(n)$ , (i.e. estimate of the original source signal) is obtained by filtering the prediction error signal  $\hat{e}(n)$  through  $1/\hat{A}(z)$ .

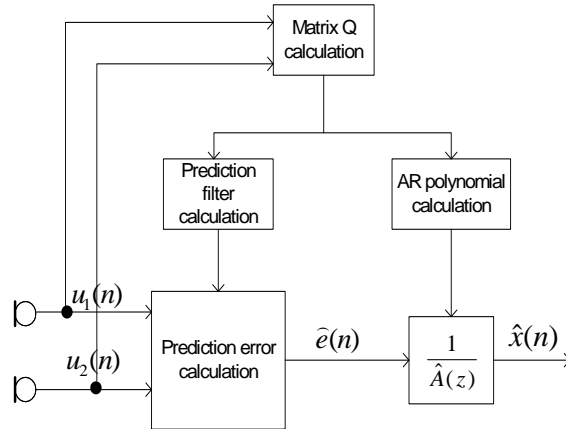


Fig. 2: Diagram of the blind dereverberation algorithm

### 3. Experimental Results and Discussion

In this section, we present results of three experiments using MRI acoustic noise as the original source signal. The reverberant signals are generated synthetically for the first experiment while the actual microphone measurements in a test-room and in a test-bed are used in the second and third experiments. We also introduce a criterion based on the power spectra of the original and dereverberated (recovered) signals in order to evaluate performance of the method in our experiments. The performance criterion, called DPS (Distortion of Power Spectrum), is defined as

$$DPS = \frac{1}{M} \sum_{m=0}^{M-1} \left| 10 \lg |P(m)| - 10 \lg |\hat{P}(m)| \right| \quad (14)$$

where,  $m$  denotes frequency index,  $P(m)$  and  $\hat{P}(m)$  are the PSD (Power Spectrum Density) samples of the original signal and the dereverberated signal, respectively. We also use the above criteria to obtain  $\hat{A}(z)$  of optimal order giving minimum value for the DPS in our experiments.

#### 3.1. Experiment 1

In this experiment we generate the reverberant signals from the original MRI noise signal synthetically. We use the Image Method [18] to generate the RTFs  $H_1(z)$  and  $H_2(z)$  for two acoustic paths, as shown in the flowchart of Fig. 3. Input to these RTFs is the original signal  $x(n)$ . Output of each RTF is a distorted version of the original signal representing the reverberant signal  $u_i(n)$ , for  $i=1,2$ , measured by the microphones. We refer to the measurements of  $u_1(n)$  and  $u_2(n)$  as synthetic (reverberant) data. Test-room parameters used in generating the RTFs are: (1) Room size:  $2.90 \times 4.65 \times 2.74 \text{ m}^3$ ; (2) Noise source position  $(x, y, z)$ :  $(0.50, 3.74, 0.80) \text{ m}$ ; (3) Receiver 1 (i.e. Microphone 1,  $M_1$ ) position:  $(1.94, 2.11, 0.85) \text{ m}$ ; (4) Receiver 2 (i.e. Microphone 2,  $M_2$ ) position:  $(1.35, 0.97, 0.85) \text{ m}$ ; and (5) Absorption coefficients: wall and ceiling: 0.7, floor: 0.3. The test-room size and positions of the loudspeaker and microphones are exact measurements. Fig. 4 shows generated room impulse responses  $h_1(n)$  and  $h_2(n)$  for  $H_1(z)$  and  $H_2(z)$  systems, respectively. The reverberation time is approximately 100 ms. Each impulse response is truncated to 3000. System parameters used in this simulation are as follows: sampling rate: 32 kHz, order of each prediction filter:  $L = 100$ , order of AR process model:  $N=2L= 200$ , length of measured data: 60000 samples. The order  $L$  was varied, and  $L = 100$  was selected for smallest value of DPS in (14) during our experimentation. We use data samples of  $u_1(n)$  and  $u_2(n)$  in our blind dereverberation algorithm to obtain  $\hat{A}(z)$  and  $\hat{x}(n)$  - the dereverberated signal.

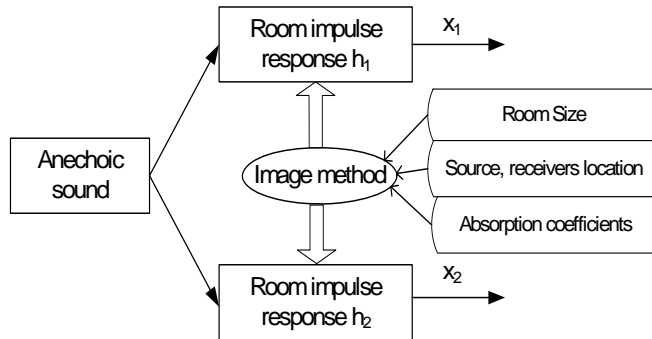


Fig.3: Diagram for generating reverberant signals using Image method

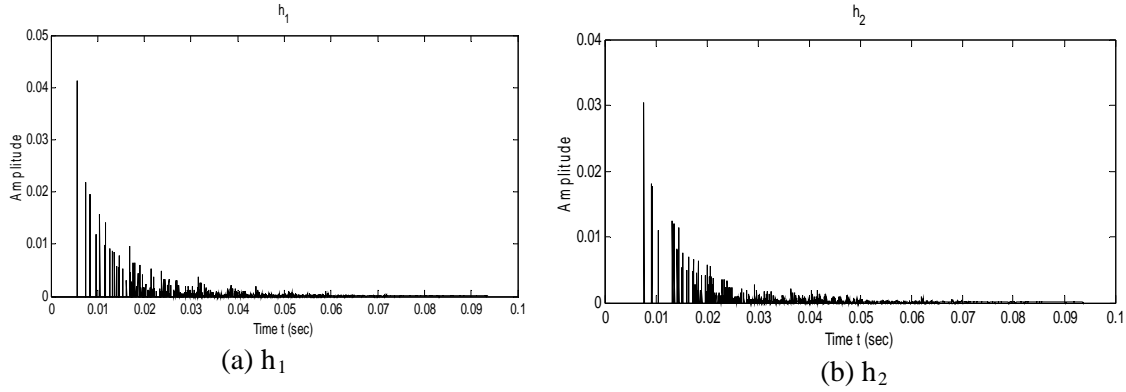
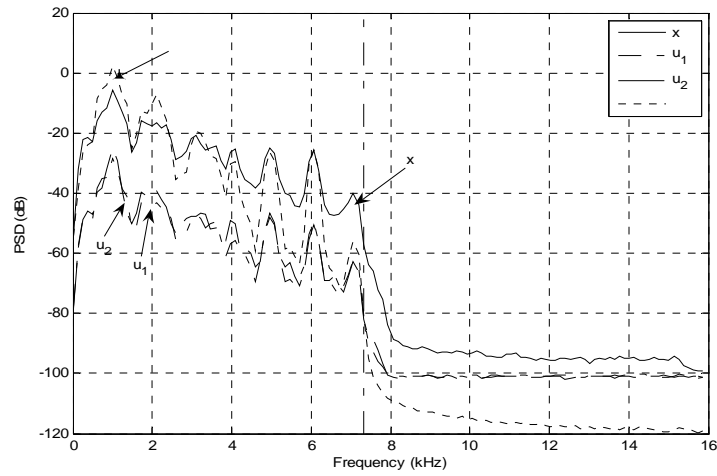
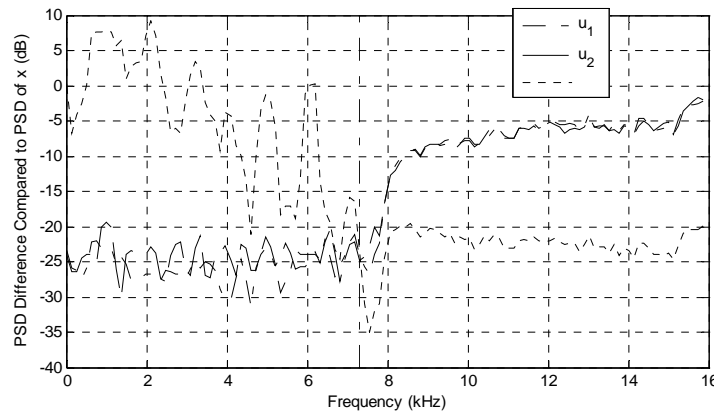


Fig. 4 Experiment 1 - Room impulse responses generated by Image Method

Note that MATLAB routines may give numerically inaccurate values when calculating the characteristic polynomial of a large size matrix  $\mathbf{Q}$  (e.g. 200 by 200), leading to an unstable  $1/\hat{A}(z)$ , as it was experienced by us. Because of this, we had to adapt and use an efficient and numerically robust algorithm given originally in [19]. Fig. 9 shows flowchart of the algorithm we used. In this algorithm, the matrix is upper diagonalized after Hessenberg Transformation. Figures 5(a) and 5(b) illustrate PSD of the signals and the differences between the recovered (dereverberated) signal with the original and reverberant signals. It is easy to see that significant attenuation of the reverberation has been reached, and that the recovered signal shows good estimation of the original signal within 7.3KHz bandwidth suppressing the signal components from 7.3KHz to 16KHz. 7.3 kHz is the approximate bandwidth of the measured MRI acoustic noise signal. This effect demonstrates that AR process is a proper model for MRI noise signal instead of background noise. Therefore by applying the estimated AR filter, the background noise beyond the MRI noise signal band is suppressed. In this experiment using the criterion in (14), we obtain DPS values of 24.26dB, 25.60dB, and 7.98dB for  $u_1(n)$ ,  $u_2(n)$  and  $\hat{x}(n)$  versus the original signal, respectively. That means reverberation in  $u_1(n)$  and in  $u_2(n)$  are reduced by 16.28dB and 17.62dB in the recovered signal  $\hat{x}(n)$ , respectively.



(a)



(b)

Fig. 5: Experiment 1 - (a) PSD of original signal  $x(n)$ , Microphone output  $u_1(n)$ ,  $u_2(n)$  and recovered signal  $\hat{x}(n)$  in synthetic simulation; (b) PSD difference of  $u_1(n)$ ,  $u_2(n)$  and  $\hat{x}(n)$  compared to  $x(n)$ .

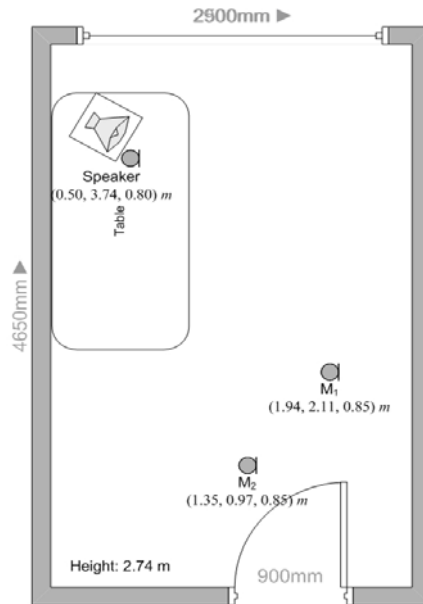
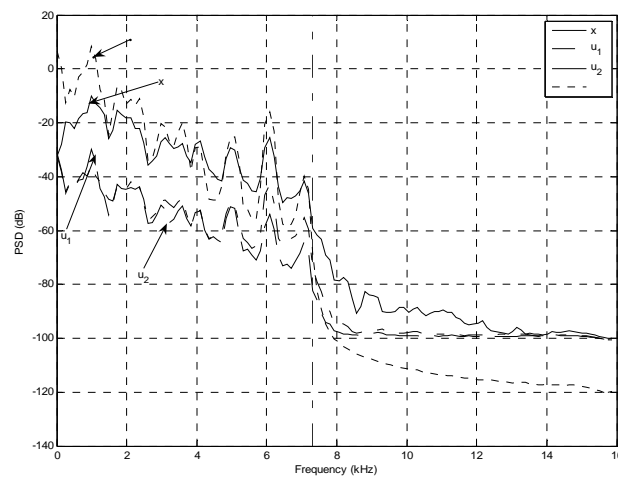
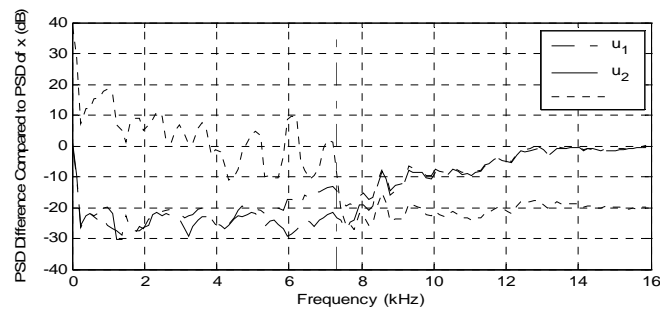


Fig. 6: Test-room layout



(a)



(b)

Fig. 7: Experiment 2 - (a) PSD of original signal  $x(n)$ , microphone output  $u_1(n)$ ,  $u_2(n)$  and recovered signal  $\hat{x}(n)$ ; (b) PSD difference of  $u_1(n)$ ,  $u_2(n)$  and  $\hat{x}(n)$  compared to  $x(n)$ .

### 3.2. Experiment 2

To evaluate performance of the algorithm in real environments, we conduct the second experiment on the reverberant MRI noise recorded in a test-room. Fig. 6 shows layout of the test-room and the positions of microphones and a broadband loudspeaker generating the original signal (the MRI actual noise).

In addition to a high-speed computer, the system setup includes: (i) software graphical design package (Labview 8.20), (ii) data acquisition card (NI-PCI4472), (iii) loudspeaker (BIC 52-SI, 8-Ohm, 2-way 6-inch woofer and 0.75-inch tweeter, 43 to 20,000Hz, 150Watts, bookshelf size:  $24 \times 17.5 \times 12.2$  inches), and (iv) microphones (B&K 2669C, polarized diffuse-field). Considering the influence of sound card, amplifier and speaker to the original signal, we place one microphone very close to the loudspeaker. The output of this microphone is assumed to be the clean signal without reverberation, i.e. the original signal  $x(n)$ . Two other microphones record the reverberant signals,  $u_1(n)$  and  $u_2(n)$ . We take the measured signals  $u_1(n)$  and  $u_2(n)$  as the inputs to our algorithm in order to estimate  $x(n)$  by  $\hat{x}(n)$  as what was done in Experiment 1. Fig. 7 shows PSD and its difference among the original (MRI noise), reverberant, and recovered signals in the 7.3KHz bandwidth. As expected for the real experiments, the performance has degraded and the estimated signal  $\hat{x}(n)$  is not as good as it was in Experiment 1. However, we should point out that  $u_1(n)$  and  $u_2(n)$  are different from those generated analytically in Experiments 1. Recorded reverberant signals display some modulation effect that remains in the recovered signal in this experiment. In Experiment 1, the reverberant signals  $u_1(n)$  and  $u_2(n)$  are obtained via the RTFs  $H_1(z)$  and  $H_2(z)$  free from such modulation effect. In this experiment, we obtain DPS values for  $u_1(n)$ ,  $u_2(n)$  and  $\hat{x}(n)$  as 21.15 dB, 23.91 dB, and 8.00 dB, respectively. These results show that the reverberations shown in  $u_1(n)$  and  $u_2(n)$  are reduced by 13.15 dB and 15.91dB in the recovered signal  $\hat{x}(n)$ , respectively.

### 3.3. Experiment 3

In this experiment, we aim at evaluating the performance of our blind dereverberation method in a test-bed which is manufactured to mimic the MRI bore. As shown in Fig. 8, the test-bed consists of a half cylinder made of transparent acrylic (thickness 2.5cm) mounted on a plywood base (thickness 2.5 cm). The dimensions of the structure are length 1.5 m (5 feet) and diameter 0.76 m (2.5 feet) similar to the dimensions of the 3T-Siemens MRI bore. The thickness of the test-bed walls were chosen to minimize vibration, yet leaving the test-bed portable. The test-room dimensions are 4.5 m (L)  $\times$  2.8 m (W)  $\times$  2.6 m (H). A full-size manikin inside the bore imitates a human body.

Original signal is the actual MRI acoustic noise fed to a broadband loudspeaker producing the source noise in the test-bed cavity. We place the loudspeaker in one end of the test-bed cavity (on the foot-side of manikin). The microphones  $M_1$  and  $M_2$  are positioned near manikin's head (ears), slightly asymmetrical with respect to the loudspeaker, on the other side of the test-bed cavity. Although this setup does not exactly match the model of noise source in real MRI bore, it will allow us to place the microphones inside the test-bed cavity conveniently away from the damaging effects of strong magnetic field gradient present in real MRI machine. This setup will also provide us with the level of reverberation created in an acoustic cavity similar in size to the real MRI bore. Computed DPS values for  $u_1(n)$ ,  $u_2(n)$  and  $\hat{x}(n)$  are 3.97dB, 4.36dB, and 2.85dB, respectively. These results show that the spectral distortion due to reverberation is rather low in both  $u_1(n)$  and  $u_2(n)$  in comparison with those obtained in Experiment 1 and 2. We attribute presence of low reverberation levels to small (volume) size of the test-bed bore. The reverberation level of  $u_1(n)$  and  $u_2(n)$  are reduced by 1.12 dB and 2.51dB in  $\hat{x}(n)$ , respectively.



Fig. 8: Experiment 3 - Test-bed mimicking the MRI bore

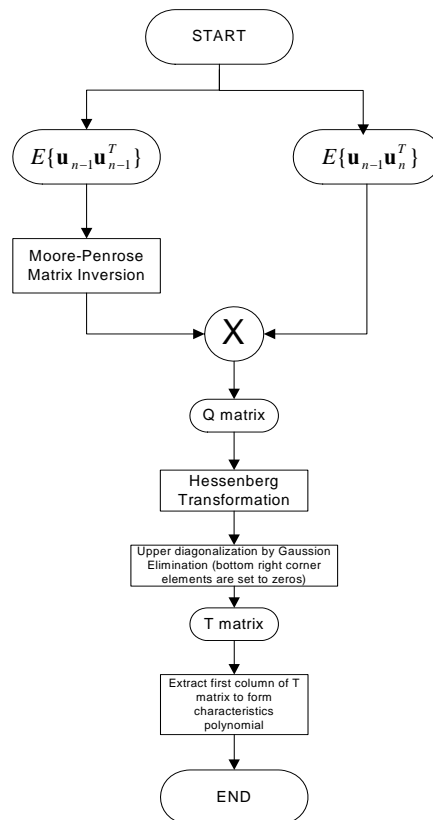


Fig. 9: Flowchart for computing  $Q$  and its characteristic polynomial.

## 4. Conclusion

Reverberation degrades the performance of ANC method for MRI acoustic noises. There is demand to verify the effectiveness of dereverberation for MRI acoustic noises and MRI environment. We apply the LIME method to conduct blind dereverberation on reverberant MRI noises. Also, we define DPS, a quantitative criterion comparing the power spectrum of the original noise source and the estimated one to evaluate the dereverberation performance. We consider three types of reverberant signals: synthetic signal using image method, recorded signal in test room, and MRI bore test-bed. The purpose of the third experiment is to mimic the MRI bore. Results show that reverberation is reduced by 16.28 dB, 13.15 dB, and 1.12 dB in the three experiments, respectively. In the third experiment, the reverberation distortion is much smaller than the other two due to small volume of the MRI bore test-bed, which also cause the amount the reverberation improvement to be much less than those in the other two experiments. In the mean time, the environmental noise is suppressed significantly. The results demonstrated the effectiveness of the blind dereverberation algorithm in realistic environments. Future work includes reducing computational complexity for real-time implementation, increasing the number of microphones in order to improve the performance, and combining the dereverberation algorithm with ANC method for achieving better attenuation of MRI noise.

## 5. Acknowledgement

This study was supported by the VA IDIQ contract number VA549-P-0027 awarded and administered by the Dallas, TX VA Medical Center. The content of this paper does not necessarily reflect the position or the policy of the U.S. government, and no official endorsement should be inferred.

## 6. References

- [1] A. Moelker and P. M. T. Pattynama, "Acoustic noise concerns in functional magnetic resonance imaging," *Human Brain Mapping*, vol. 20, pp. 123-141, 2003.
- [2] D. Tomasi, E. C. Caparelli, L. Chang and T. Ernst, "fMRI-acoustic noise alters brain activation during working memory tasks," *Neuroimage*, vol. 27, pp. 377-386, 8/15. 2005.
- [3] T. Miyati, T. Banno, H. Fujita, M. Mase, H. Narita, M. Imazawa and S. Ohba, "Acoustic noise analysis in echo planar imaging: multicenter trial and comparison with other pulse sequences," *Medical Imaging, IEEE Transactions on*, vol. 18, pp. 733-736, 1999.
- [4] M. E. Ravicz and J. R. Melcher, "Isolating the auditory system from acoustic noise during functional magnetic resonance imaging: examination of noise conduction through the ear canal, head, and body," *J. Acoust. Soc. Am.*, vol. 109, pp. 216, 2001.
- [5] S. M. Kuo and D. R. Morgan, "Active noise control: a tutorial review," *Proc IEEE*, vol. 87, pp. 943-973, 1999.
- [6] M. McJury, R. W. Stewart, D. Crawford and E. Toma, "The use of active noise control (ANC) to reduce acoustic noise generated during MRI scanning: Some initial results," *Magn. Reson. Imaging*, vol. 15, pp. 319-322, 1997.
- [7] M. Li, T. C. Lim and J. Lee, "Simulation study on active noise control for a 4-T MRI scanner," *Magn. Reson. Imaging*, vol. 26, pp. 393-400, 4. 2008.
- [8] M. H. Lu and P. M. Clarkson, "The performance of adaptive noise cancellation systems in reverberant rooms," *J. Acoust. Soc. Am.*, vol. 93, pp. 1122, 1993.
- [9] Q.G. Liu, B. Champagne and P. Kabal, "Room speech dereverberation via minimum-phase and all-pass component processing of multi-microphone signals", *IEEE Pacific Rim Conference on Communications, Computers, and Signal Processing, Proceedings of*, pp. 571-574, May, 1995.

- [10] J. Ma and D.J. Pines, "Dereverberation and its application to damage detection in one-dimensional structures", *American Institute of Aeronautics and Astronautics Journal*, Vol. 39, No. 5, pp.902-918., 2001.
- [11] C. Samson and G.F. West, "Dereverberation of marine reflection seismic data by a spatial combination of predictive deconvolution and velocity filtering", *Journal of Marine Geophysical Researches*, vol. 17, pp.1-15, 1993.
- [12] D. Erdogmus, K.E. Hild, J.C. Principe, M. Lazaro and I. Santamaria, "Adaptive blind deconvolution of linear channels using Renyi's entropy with Parzen window estimation", *IEEE Transactions on Signal Processing*, vol. 52, No. 6, pp.1489-1498, 2004.
- [13] J.C. Principe, H.C. Wu, "Blind separation of convolutive mixtures", *International Joint Conference on Neural Networks*, July 10-16, 1999.
- [14] T. Hikichi, M. Delcroix and M. Miyoshi, "Inverse Filtering for Speech Dereverberation Less Sensitive to Noise and Room Transfer Function Fluctuations", *EURASIP Journal on Advances in Signal Processing*, Vol 2007, Article ID 34013, 12 pages, 2007.
- [15] A. Chan and H. Leung, "Inverse filtering of room acoustics using a nonlinear dynamical approach", *IEEE International Conference on Communications*, vol.2, pp.1110-1114, Jun. 1997.
- [16] M. Delcroix, T. Hikichi, and M. Miyoshi, "Blind dereverberation algorithm for speech based on multi-channel linear prediction", *Acoust. Sci. & Tech.*, Vol.26, No. 5, pp. 432-439, Jan. 2005
- [17] H. Bao, I. M. S. Panahi and R. Briggs, "Blind Dereverberation for fMRI Noise Based on SIMO Linear Prediction Method," *29th Annual International Conference of the IEEE Engineering in Medicine and Biology Society*, pp. 2831-2834, Lyon, France, Aug. 23-26, 2007
- [18] J.B. Allen and D.A. Berkeley, "Image method for efficiently simulating small-room acoustics", *J. Acoust. Soc. of America.*, Vol.65, No.4, pp.943-950, Apr. 1979.
- [19] S. Rombouts and K. Heyde, "An accurate and efficient algorithm for the computation of the characteristic polynomial of a general square matrix", *J. Comput. Phys.*, vol. 140, pp. 453-458, 1998.